Cellular Response to Magnetic Nanoparticles "PEGylated" via Surface-Initiated Atom Transfer Radical Polymerization

Feixiong Hu, Koon Gee Neoh,* Lian Cen, and En-Tang Kang

Department of Chemical and Biomolecular Engineering, National University of Singapore, Kent Ridge, Singapore 119260

Received November 16, 2005; Revised Manuscript Received January 15, 2006

A new method to PEGylate magnetic nanoparticles with a dense layer of poly(poly(ethylene glycol) monomethacrylate) (P(PEGMA)) by surface-initiated atom transfer radical polymerization (ATRP) is reported. In this approach, an initiator for ATRP was first immobilized onto the magnetic nanoparticle surface, and then P(PEGMA) was grafted onto the surface of magnetic nanoparticle via copper-mediated ATRP. The modified nanoparticles were subjected to detailed characterization using FTIR, XPS, and TGA. The P(PEGMA)-immobilized nanoparticles dispersed well in aqueous media. The saturation magnetization values of the P(PEGMA)-immobilized nanoparticles were 19 emu/g and 11 emu/g after 2 and 4 h polymerization respectively, compared to 52 emu/g for the pristine magnetic nanoparticles. The response of macrophage cells to pristine and P(PEGMA)-immobilized nanoparticles was compared. The results showed that the macrophage cells are very effective in cleaning up the pristine magnetic nanoparticles. With the P(PEGMA)-immobilized nanoparticles, the amount of nanoparticles internalized into the cells is greatly reduced to <2 pg/cell over a 5 day period. With this amount of nanoparticles uptake, no significant cytotoxicity effects were observed.

1. Introduction

Magnetic nanoparticles have been deemed to have great potential in in-vivo biomedical applications including magnetic resonance imaging (MRI) contrast enhancement,[1−4] targeted drug delivery,[5,6] hyperthermia,[7] and magnetic field assisted radionuclide therapy.[8] Because of their large surface area/volume ratio, nanometer-sized iron oxide cores tend to agglomerate into large clusters and adsorb plasma proteins. When nanoparticles agglomerate or are covered with adsorbed plasma proteins, they not only lose the specific properties associated with their nanometer dimensions, but they can also be quickly cleared by macrophages and be accumulated in the reticuloendothelial system before they can reach the target cells.[9]

One possible approach to increase the circulation time of nanoparticles in the blood stream is to modify the particles with poly(ethylene glycol) (PEG). Surfaces covered with PEG have proven to be nonimmunogenic, nonantigenic, and protein resistant.[10,11] Immobilization of PEG macromolecules on iron oxide for biocompatibility has been achieved via a "grafting to" technique.[12,13] However, this technique often leads to low grafting density and low film thickness, as the polymer molecules must diffuse through the existing polymer film to reach the reactive sites on the surface. Furthermore, each surface-immobilized PEG macromolecule has only one site available for ligand coupling which limits their utility for further functionalization, such as protein grafting.[14] In contrast, a "grafting from" approach would be more suitable for achieving highly stable polymer layer and high graft density.[15] Progress in polymer synthesis techniques, such as atom transfer radical polymerization (ATRP) and reversible addition−fragmentation chain transfer (RAFT)-mediated polymerization, also makes it possible to produce polymer chains with controllable lengths. Furthermore, surface-initiated polymerization of poly(ethylene glycol) monomethacrylate (PEGMA) onto the surface of iron oxide offers more sites for ligand coupling as each monomer has one active site.

$MnFe_2O_4$ and Fe_2O_3 core/polystyrene shell nanoparticles have been synthesized via ATRP technique where linear polymeric molecules attach to the surface of metal oxide cores through linker molecules (the initiator) via the −COOH group.[16,17] However, this noncovalent linkage cannot offer a permanent linkage for hydrophilic polymers. In a biological system, the hydrophilic polymer chains will be extended, and a dynamic exchange between the polymeric chain and other competing molecules possessing −COOH groups such as peptides and amino acids in the biological system could lead to the dissociation of the polymeric chains from the core surfaces. To solve this problem, divinylbenzene was employed for cross-linking the linear polymer chains to improve the stability of the core/shell nanoparticles.[18] However, in such a system, cross-linking of polymer chains from different particles by divinylbenzene would also take place which leads to aggregation of the particles.

In this work, we applied a copper-mediated ATRP technique to graft polymerize PEGMA on Fe_3O_4 nanoparticles via a silane initiator, [4-(chloromethyl)phenyl]trichlorosilane (CTS) (Figure 1). In an earlier work, another silane initiator, 2-(4-chlorosulfonylphenyl) ethyltrichlorosilane, was used for ATRP of methyl methacrylate on magnetic nanoparticles.[19] However, we could not use this initiator for PEGMA, probably due to its reaction with the PEGMA monomer. Poly(poly(ethylene glycol) monomethacrylate) (P(PEGMA)) has been used to conjugate with proteins to increase their plasma half-lives and stability.[20,21] It has also been used to functionalize surfaces to increase their tissue and blood compatibility and to increase their resistance to protein fouling.[22−24] Hence, we expect the following advantages from the PEGylation of nanoparticles with P(PEGMA) via ATRP: higher polymer density on the particle surface, controllable molecular weight, and more active groups for further functionalization. Uptake of P(PEGMA) functionalized

* Corresponding author. Tel: +65 68742176. Fax: +65 67791936. E-mail: chenkg@nus.edu.sg.

10.1021/bm050870e CCC: $33.50
Published on Web 02/15/2006

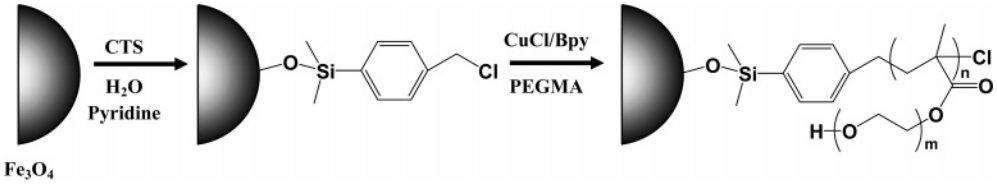

Figure 1. Schematic representation for the preparation of PEGMA-coated magnetic nanoparticle by surface-initiated ATRP.

nanoparticles by macrophage cells was also compared to that of the pristine Fe_3O_4 nanoparticles to evaluate the applicability of this technique for increasing in-vivo half-life of magnetic nanoparticles.

2. Materials and Methods

2.1. Materials. Benzyl ether, 1,2-hexadecanediol, oleic acid, oleylamine, iron(III) acetylacetonate, [4-(chloromethyl)phenyl]trichlorosilane (CTS), 2, 2′-bipyridyl (Bpy), and copper(I) chloride were purchased from Aldrich Chemical Co. and used as received. Pyridine was dried over potassium hydroxide and distilled before use. Toluene was dehydrated with 4 Å molecular sieves before use. Poly(ethylene glycol) monomethacrylate (PEGMA) macromonomer ($M_n \sim 360$) was passed through a silica gel column to remove the inhibitor and stored under an argon atmosphere at −10 °C. Mouse macrophage cells (RAW 264.7) were purchased from ATCC. RPMI-1640 medium, fetal bovine serum, L-glutamine, penicillin, and streptomycin were purchased from Sigma. All other solvents and chemicals were purchased from either Fisher Scientific or Aldrich and used as received.

2.2. Preparation of Magnetic Nanoparticles. The Fe_3O_4 magnetic nanoparticles were prepared according to a reported method:[25] iron(III) acetylacetonate (5 mmol), 1,2-hexadecanediol (25 mmol), oleic acid (15 mmol), oleylamine (15 mmol), and phenyl ether (50 mL) were mixed and magnetically stirred under a flow of nitrogen. The mixture was heated to 200 °C for 2 h and then, under a blanket of nitrogen, heated to reflux (300 °C) for another 1 h. The black mixture was cooled to room temperature after removal of the heat source. Under ambient conditions, ethanol (100 mL) was added to the mixture, and a black material was precipitated and separated via centrifugation. The black product was dissolved in 40 mL of hexane in the presence of oleic acid (1 mL) and oleylamine (1 mL). Centrifugation (6000 rpm, 10 min) was applied to remove any undispersed residue. The product, Fe_3O_4 nanoparticles of ~6 nm, was then precipitated with ethanol, centrifuged (6000 rpm, 10 min) to remove the solvent, and then dried under reduced pressure and stored at 0−4 °C.

2.3. Surface-Initiated Atom Transfer Radical Polymerization. The magnetic nanoparticles with the initiator, CTS, for copper-mediated ATRP were prepared by self-assembled deposition method. A total of 20 mg of nanoparticles was first dispersed in 20 mL of dry toluene, and then 200 μL of dry pyridine and 50 μL of CTS were added to the nanoparticle suspension under the protection of argon. The mixture was sonicated for 1 h, and then the flask was opened to the air and sonicated for another 2 h at room temperature. The resulting CTS-immobilized nanoparticles were isolated with a centrifuge and washed with toluene in the presence of 1% of pyridine twice to remove the residue initiator. The CTS-immobilized nanoparticles were then washed with acetone and water.

The surface-initiated polymerization of PEGMA was carried out as follows: the CTS-immobilized nanoparticles and 4 mL of deionized water were introduced into a Pyrex tube containing a magnetic stir bar. The suspension was sonicated for 10 min to get a uniform suspension and followed by the addition of 2 mL of PEGMA monomer. The mixture was purged with argon for 15 min, and then CuCl (20 mg) and Bpy (67 mg) were added. After purging with argon for another 10 min, the Pyrex tube was sealed and kept in a 30 °C water bath under stirring. After prescribed polymerization times, the reaction was stopped by adding ethanol at a solution/ethanol ratio of 1:5. The modified Fe_3O_4 nanoparticles were collected by centrifuging at a speed of 20 000 rpm. The collected nanoparticles were re-dispersed in ethanol and centrifuged at a speed of 1000 rpm for 5 min to remove any Cu(II) precipitate formed in the ATRP process. The nanoparticles were then collected by centrifuging at 20 000 rpm and subjected to repeated cycles of washing with ethanol and centrifugation to remove the unreacted monomer and homopolymer before further characterization.

2.4. Cell Culture. Mouse macrophage cells (RAW 264.7) were used to test the intracellular uptake of the magnetic nanoparticles. The cells were routinely cultured in RPMI-1640 medium, supplemented with 10% fetal bovine serum, 2 mM L-glutamine, 100 IU/mL penicillin, and 100 μg/mL streptomycin at 37 °C in 5% CO_2 atmosphere. The cultured cells were washed with PBS and detached with trypsin−EDTA solution. The cells were then collected by centrifugation and resuspended with the medium containing nanoparticles at a concentration of 0.2 mg/mL to achieve a cell concentration of 10^5 cells/mL. The cells were then seeded in 24-well culture plates. In the control experiment, the cells were cultured in the medium at the same cell concentration but without magnetic nanoparticles. After incubation at 37 °C for prescribed time periods, the cells were washed with PBS three times to remove the nanoparticles in the medium and were detached with trypsin−EDTA solution. After counting with a hemocytometer, the cells were collected by centrifugation, and the cell pellet was dissolved in 37% HCl at 60 °C for 2 h. The iron concentration was determined using inductively coupled plasma−mass spectroscopy (ICP-MS, Perkin-Elmer Elan 6100).

2.5. Characterization. FTIR spectra were obtained in a transmission mode on a Bio-Rad FTIR spectrophotometer (Model FTS135) under ambient conditions. The samples of pristine and functionalized Fe_3O_4 nanoparticles were ground with KBr and then compressed into pellets. The spectrum was taken from 400 to 4000 cm^{-1}. Typically, 64 scans at a resolution of 8 cm^{-1} were accumulated to obtain one spectrum.

The chemical composition of the pristine and the functionalized magnetic nanoparticles was determined with X-ray photoelectron spectroscopy (XPS) on an AXIS HSi spectrometer (Kratos Analytical Ltd.) using a monochromatized Al Kα X-ray source (1486.6 eV photons) at a constant dwell time of 100 ms and a pass energy of 40 eV. The anode voltage was 15 kV, and the anode current was 10 mA. The pressure in the analysis chamber was maintained at 6.7×10^{-6} Pa or lower during each measurement. The nanoparticles were mounted on standard sample studs by means of double-sided adhesive tape. The core-level signals were obtained at a photoelectron takeoff angle of 90° (with respect to the sample surface). To compensate for surface charging effect, all core-level spectra were referenced to the C 1s hydrocarbon peak at 284.6 eV. In spectral deconvolution, the line width (full width at half-maximum) of the Gaussian peaks was maintained constant for all components in a particular spectrum. The peak ratios for various elements were corrected using experimentally determined instrumental sensitivity factors.

Thermogravimetric analysis (TGA) data were obtained with a TGA 2050 thermogravimetric analyzer (TA Instruments). Samples weighing between 5 and 15 mg were heated from 30 to 700 °C at a heating rate of 10 °C/min in air. The transmission electron microscopy (TEM) images were recorded on a JEOL 2010 transmission electron microscope at an accelerating voltage of 200 kV. The TEM specimens were made by placing a drop of the nanoparticle suspension on a carbon-coated copper grid. Measurement of magnetization was carried out with a vibrating sample magnetometer (VSM) (Model 1600, DMS). The hydrodynamic size of the P(PEGMA)-immobilized magnetic nanoparticles was determined by dynamic light scattering using a 90 Plus

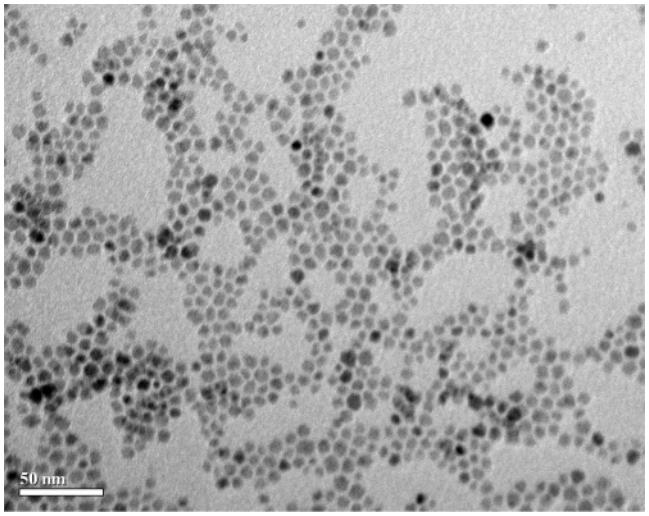

Figure 2. TEM image of the pristine magnetic nanoparticles with oleic acid coating.

particle size analyzer (Brookhaven Instruments). The molecular weight of the P(PEGMA) brushes grafted on the magnetic nanoparticle surface was determined by gel permeation chromatography (GPC). The P(PEGMA)-immobilized nanoparticles sample was first dissolved in 10% HF for 5 h. Then 1 M NaOH was used to neutralize the HF. After freeze-drying, the polymer was redissolved in tetrahydrofuran (THF) and centrifuged to remove the salts. The polymer was recovered after removal of the THF under reduced pressure and the molecular weight measurement was performed on a Waters Breeze GPC equipped with a Waters 1515 HPLC pump and a Waters 2414 refractive index detector, using poly(ethylene glycol) as the calibration standard. Water was used as the eluent at a flow rate of 1 mL/min.

3. Results and Discussion

3.1. Physical Properties of the Magnetic Nanoparticles. Magnetic particles obtained under different synthetic conditions may display very different properties, such as particle size, shape, composition, magnetic properties, and so on. In the present work, the Fe_3O_4 magnetic nanoparticles were synthesized via high-temperature organic phase decomposition of an iron precursor, and the TEM image of these nanoparticles is shown in Figure 2. It can be seen from Figure 2 that the particles are quite uniform with a particle size of 6.2 ± 0.7 nm. The magnetic nanoparticles disperse well in organic solvents due to the presence of oleic acid on the particle surface. The aggregation of the nanoparticles seen in Figure 2 arises during the evaporation of the organic solvent, where the nanoparticles aggregated together to reduce their surface energy in the atmosphere.

The saturation magnetization value of the nanoparticles as determined by the VSM is 52 emu/g at 25 °C (Figure 3a). After correcting for the oleic acid content (~26%), the saturation magnetization value is 70 emu/g of Fe_3O_4, which is lower than the bulk magnetite value of 90 emu/g.[26] This reduction in magnetization may be the result of noncollinear spins at the nanoparticle surface. From Figure 3a, no hysteresis curve was observed which indicates the characteristic superparamagnetic behavior of the nanoparticles under room temperature, i.e., the nanoparticles would not retain any magnetism after removal of the magnetic field. These nanoparticles with superparamagnetic property have been used as MR T_2 contrast agents. Each of these small superparamagnetic nanoparticles contains a single magnetic domain. In their natural state, the magnetic moments of these magnetic domains are oriented randomly, but in the presence of an external magnetic field, magnetic moments of these domains are aligned along the field. As a result, magnetic susceptibility of a system with such nanoparticles usually far exceeds that of paramagnetic materials, such as Gd chelate, which are widely used as T_1 contrast agents.[27]

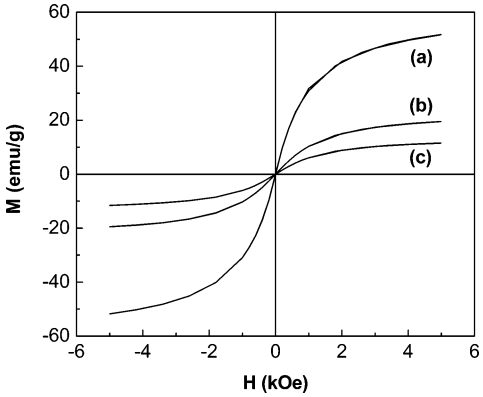

Figure 3. Field dependent magnetization at 25 °C for (a) pristine magnetic nanoparticles and (b, c) P(PEGMA)-immobilized nanoparticles after polymerization time of 2 and 4 h, respectively.

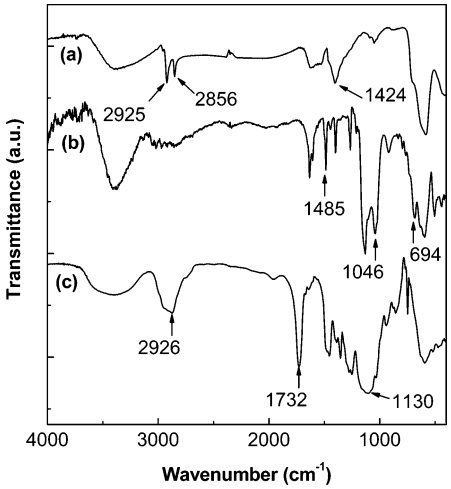

Figure 4. FTIR spectra of (a) pristine magnetic nanoparticles, (b) CTS-immobilized nanoparticles, and (c) P(PEGMA)-immobilized nanoparticles after polymerization time of 4 h.

3.2. Surface-Initiated ATRP of PEGMA. The chemical composition of the pristine and CTS-immobilized nanoparticles was analyzed by FTIR (Figure 4). The FTIR spectrum of the pristine magnetic nanoparticles (Figure 4a) exhibits strong bands in the low-frequency region (at 410 and 580 cm^{-1}) due to the iron oxide skeleton, which are highly consistent with the spectrum of magnetite.[28,29] The spectrum also shows characteristic absorption bands of oleic acid on the magnetic nanoparticle surface, such as that at 1424 cm^{-1} for alkanes and at 2856 and 2925 cm^{-1} for CH_2 groups.[30] However, from Figure 4a, the symmetric COO^- stretch band at 1410 cm^{-1} cannot be differentiated from the 1424 cm^{-1} band. Similarly, the 1540 cm^{-1} band due to the asymmetric COO^- stretch is not clearly discernible. The C═O stretching frequency of the oleic acid ligand usually at ~1700 cm^{-1} is also not observed in the spectrum. This absence can be attributed to the bonding of the oleic acid ligand to the nanoparticle surface through the COO^- functionality. Similar results of the "missing" band at ~1700 cm^{-1} were also observed for *para*-substituted benzoic acid adsorbed on $MnFe_2O_4$ nanoparticles.[31] The FTIR spectrum of CTS-immobilized nanoparticles (Figure 4b) shows a band at 1046 cm^{-1} attributed to the characteristic Si−O stretch absorp-

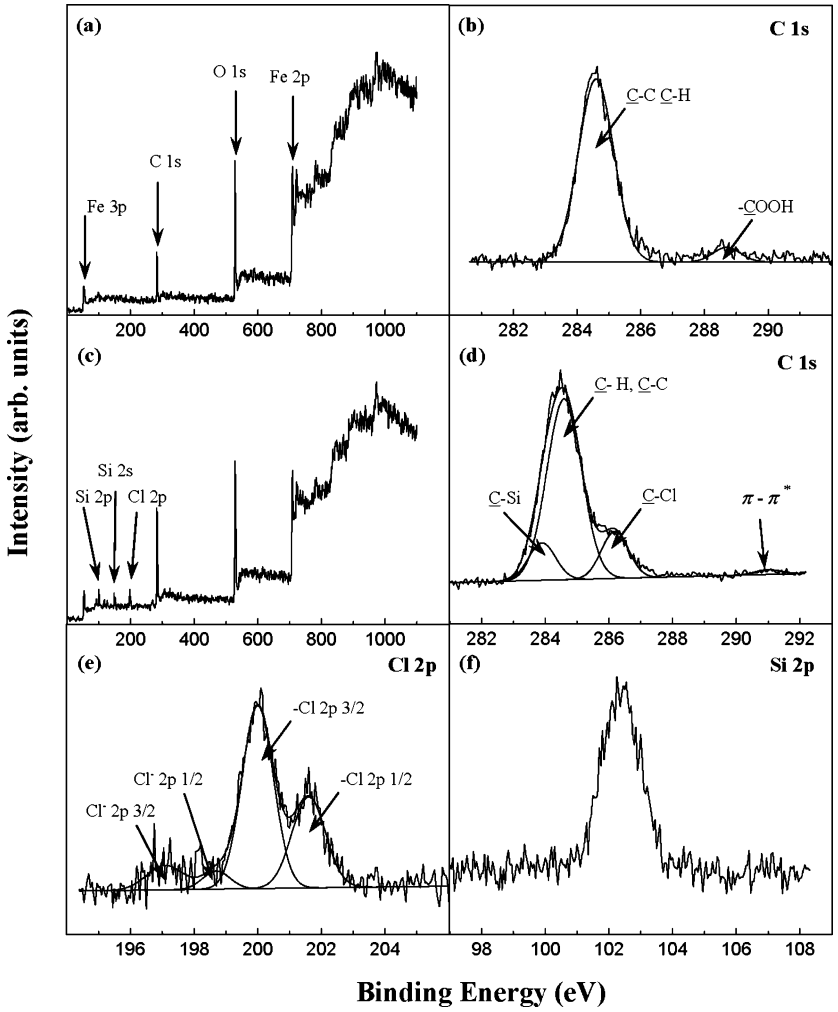

Figure 5. (a, b) XPS wide scan and C 1s core level spectra of pristine magnetic nanoparticles; (c−f) XPS wide scan and C 1s, Cl 2p, and Si 2p core level spectra of CTS-immobilized nanoparticles.

tion.[32] The band at 694 cm^{-1} can be assigned to the CH_2 group on the CTS, and the band at 1485 cm^{-1} can be assigned to the benzene ring.[30] The disappearance of the bands observed in the pristine Fe_3O_4 spectrum mentioned above is due to the reaction of Si−Cl in CTS with the −COOH group of oleic acid which results in displacement of oleic acid from the surface of the magnetic nanoparticles into the solution. The FTIR spectrum of the magnetic nanoparticles modified with P(PEGMA) (Figure 4c) shows a broad band at 1130 cm^{-1} attributed to the C−O−C ether stretch band, and a band at 1732 cm^{-1} assigned to the stretch band of C═O. The spectrum also displays a strong band around 2912 cm^{-1} corresponding to the CH_2 stretching vibrations. The CH_2, C−O−C, and C═O absorption bands provide strong evidence that the magnetic nanoparticles have been modified with PEGMA. No strong absorption band at around 1630 cm^{-1}, which is the characteristic band for C═C stretching vibration of the PEGMA monomer, can be found from Figure 4c. The absence of C═C stretching vibration further confirms the graft polymerization of the PEGMA monomer on the magnetic nanoparticles.

Immobilization of CTS on the surface of magnetic nanoparticles is also confirmed with XPS. The photoelectron lines at binding energy (BE) of about 53, 284, 530, and 710 eV which are attributed to Fe 3p, C 1s, O 1s, and Fe 2p, respectively, are observed in the wide scan spectrum of the pristine magnetic nanoparticles (Figure 5a). Two peak components are observed in the C 1s core-level spectrum of the pristine magnetic nanoparticles. The peak at about 284.6 eV is attributed to C−C and C−H, and the peak at 288.7 eV is attributed to COOH. The area ratio of the two peaks is 16.4:1 which is close to the theoretical ratio of 17:1 for oleic acid (Figure 5b), indicating that the magnetic nanoparticle is well covered with the oleic acid layer. In addition to the photoelectron lines in Figure 5a, another three photoelectron lines at BE about 100, 150, and 200 eV which can be attributed to Si 2p, Si 2s, and Cl 2p are observed in the wide scan spectrum of CTS-immobilized nanoparticles (Figure 5c). The C 1s core-level spectrum of CTS-immobilized nanoparticles can be curve-fitted with three peak components having BE at about 283.9, 284.6, and 286.2 eV, attributable to the C−Si, C−C/C−H, and C−Cl species, respectively. The area ratio of the three peaks is 0.9:4.9:1. The $\pi-\pi^*$ shake-up satellite associated with the aromatic ring of CTS is also discernible at a BE of about 291 eV (Figure 5d). The appearance of the C−Si and C−Cl species, as well as the $\pi-\pi^*$ shake-up satellite, confirms the presence of CTS immobilized on the nanoparticles surface. Figure 5e shows the Cl 2p spectrum of CTS-immobilized nanoparticles surface, where the peak components at about 200 and 201.6 eV are assigned to C−Cl $2p_{3/2}$ and C−Cl $2p_{1/2}$, respectively. The doublet at about 197.1 and 198.7 eV is assigned to Cl^- $2p_{3/2}$ and Cl^- $2p_{1/2}$. The presence of a small amount of Cl^- ions on the nanoparticle surface can be attributed to the adsorption of Cl^- from CTS onto the nanoparticle surface. Figure 5f shows the Si 2p spectrum of the CTS-immobilized nanoparticles. The [Si]:[C]

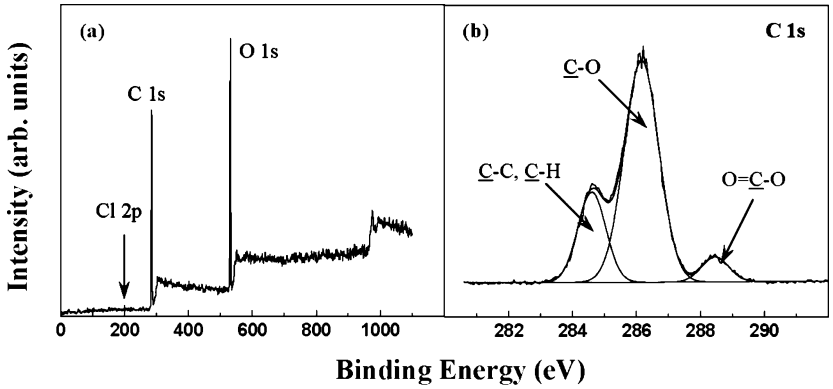

Figure 6. (a) XPS wide scan and (b) C 1s core level spectra of P(PEGMA)-immobilized nanoparticles after polymerization time of 4 h.

ratio, as determined from the Si 2p and C 1s core level spectral area ratio, is about 1:7.3, which is close to theoretical value of 1:7 for CTS.

The XPS wide scan spectrum of the Fe_3O_4 nanoparticle after surface grafting with P(PEGMA) (Figure 6a) shows two prominent photoelectron lines at binding energy of about 284 and 530 eV which are attributed to C 1s and O 1s, respectively. The absence of photoelectron lines of Fe indicates that the P(PEGMA) layer immobilized on the surface of the magnetic nanoparticles is thicker than the XPS probing depth (~5 nm). The photoelectron line for copper at about 930 eV is not found in Figure 6a which indicates that the copper from CuCl used in the ATRP process is not retained on the nanoparticle. In Figure 6a, a very weak photoelectron line at BE of 200 eV is discernible. This is assigned to the preserved active chlorine groups from ATRP. The C 1s core-level spectrum of the P(PEGMA)-immobilized nanoparticles can be curve-fitted with three peak components having BE at about 284.6, 286.2, and 288.3 eV, attributable to the C−C/C−H, C−O, and O═C−O species, respectively (Figure 6b). The area ratio of the three peaks is 3.8:11.3:1, which is close to 3:12:1 expected of P(PEGMA).

The pristine magnetic nanoparticles disperse well in organic solvents such as toluene and hexane. After surface grafting with P(PEGMA), the magnetic nanoparticles can be dispersed in ethanol as well as aqueous solvents, forming a stable brown solution. No precipitation of the magnetic nanoparticles was observed even after dispersion in ethanol for 4 months. The hydrodynamic size of the P(PEGMA)-immobilized nanoparticles after 2 h polymerization was measured to be 26 ± 5 nm, which further confirms that there is minimal aggregation between these particles in aqueous media. The molecular weight (M_n) of the P(PEGMA) was determined by GPC to be 14 100 after a polymerization time of 2 h. The surface chain density of P(PEGMA) is calculated to be 0.7 chains/nm^2, which is close to the value reported for ATRP of PEGMA on Si(111) surface.[22]

TGA studies have also been carried out for the nanoparticles modified with oleic acid, CTS, and P(PEGMA). The magnetic nanoparticles after each stage of modification give their distinctive TGA curves, which provide indications of the amount of initiator and P(PEGMA) on the magnetic nanoparticles. The TGA curve of the pristine magnetic nanoparticles (Figure 7a) shows a weight loss of about 23% after the magnetic nanoparticles have been heated to 700 °C. The residue is red−brown in color, which indicates the oxidation of Fe_3O_4 to Fe_2O_3. The oxidation of Fe_3O_4 to Fe_2O_3 results in an increase in the weight of the residue. Assuming that all Fe_3O_4 has been oxidized to Fe_2O_3, the weight of organic fraction, which is mainly oleic acid (deduced from the XPS result), is calculated to account

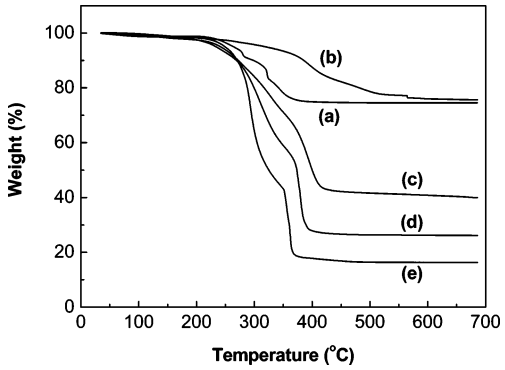

Figure 7. TGA curves of (a) pristine magnetic nanoparticles, (b) CTS-immobilized nanoparticles, and (c, d, e) P(PEGMA)-immobilized nanoparticles after polymerization time of 1, 2, and 4 h, respectively. TGA was carried out in air at a heating rate of 10 °C/min.

for 26% of the weight of the magnetic nanoparticles. The TGA curve of the magnetic nanoparticles with immobilized CTS shows a slower rate of weight loss (Figure 7b) between 200 °C and 550 °C compared to that of the pristine magnetic nanoparticles. The FTIR results have indicated that most of the oleic acid would have been displaced by CTS in the immobilization process. Hence the weight loss seen in Figure 7b would be due to the oxidation of the CTS initiator. After oxidation of the initiator molecule, the SiO_2 ash will remain in the residue. From the residual weight, it is estimated that the initiator accounts for about 33% of the weight of the CTS-immobilized nanoparticles. Parts c−e of Figure 7 show the TGA curves of P(PEGMA)-immobilized nanoparticles obtained with a polymerization time of 1, 2, and 4 h, respectively. These curves show a two-stage weight loss upon heating in air. As shown in Figure 7e, the first stage shows a weight loss of about 59% completed at 350 °C, while the second stage accounts for another 24% of the weight. This two-stage weight loss suggests that the poly(ethylene glycol) side chains are first eliminated followed by the poly(methacrylate). The amount of polymer on the magnetic nanoparticle surface increases with polymerization time. The weight loss of P(PEGMA)-immobilized nanoparticles is ~60% after 1 h polymerization and increases to ~75% after 2 h polymerization. With a 4 h polymerization time, the viscosity of the reaction mixture becomes very high as a result of the increased amount of polymer on the nanoparticle surface as well as some homopolymerization of the PEGMA in solution. The weight loss of the P(PEGMA)-immobilized nanoparticles after 4 h polymerization is ~83%. The PEGMA ATRP from the magnetic nanoparticles exhibited the characteristics of a controlled/"living" polymerization. The weight ratio of the P(PEGMA)/Fe_3O_4 calculated from the TGA results (shown in Table 1) shows

Table 1. P(PEGMA)/Fe_3O_4 Weight Ratios of CTS-Immobilized Magnetic Nanoparticles after Polymerization with PEGMA

polymerization time (h)			
0	1	2	4
0	1.52	3.15	5.51

a linear increase of polymer on the nanoparticle surface in the first 2 h, but after 2 h polymerization, this ratio is a little lower than the value expected from a linear increase. This deviation is attributed to the increasing viscosity of the mixture with polymerization time which inhibits the diffusion of the PEGMA monomer to the nanoparticle surface.

The magnetization curves of the P(PEGMA)-immobilized nanoparticles are shown in Figure 3. The saturation magnetization value can be adjusted through control of the polymerization time which in turn determines the thickness of the P(PEGMA) shell. The saturation magnetization value decreases from the 52 emu/g for the pristine nanoparticles to 19 and 11 emu/g after 2 and 4 h polymerization, respectively. On the basis of per unit weight of Fe, the average saturation magnetization values for the pristine and P(PEGMA)-immobilized particles are quite similar, at 105 ± 11 emu/(g Fe). These values are deemed sufficient for biological applications, and the magnetization values for magnetic nanoparticles coated with biocompatible substances, such as dextran, starch, gold, silica, nitriacetic acid, and PEG, have been reported to be 5−22 emu/g.[4,33−37] The grafting of PEGMA onto magnetic nanoparticle surface via ATRP has the advantages of being a controllable polymerization process and providing more reactive groups (−OH, −Cl) for further functionalization.[38] The cellular response to such functionalized magnetic nanoparticles is reported in the following section.

3.3. Cell Uptake. Figure 8 shows the optical microscopy images of macrophage cells incubated with pristine and P(PEGMA)-immobilized nanoparticles obtained after 2 h of polymerization. The macrophage cells, after culturing in the medium containing pristine magnetic nanoparticles for 1 day, are totally covered by the pristine magnetic nanoparticles (Figure 8b). A black layer of magnetic nanoparticles was formed on the bottom of the culture flask due to the precipitation of the nanoparticles in the culture medium. However, a clean area around each macrophage cell can be observed, indicating that the nanoparticles surrounding the cells were being cleaned up by the cells. After 4 days incubation, almost all the pristine magnetic nanoparticles were cleaned up by the macrophage cells (Figure 8c). This figure also shows that there was no distinct change in morphology, compared with the cells in the control experiment without nanoparticles (Figure 8a). Figure 8c also shows that the cell number has increased compared to Figure 8b. The cells incubated in the medium containing P(PEGMA)-immobilized nanoparticles after 1 day is shown in Figure 8d. Since the P(PEGMA)-immobilized nanoparticles are well dispersed in the medium, no black precipitate can be observed. The cells incubated with the P(PEGMA)-immobilized nanoparticles show similar morphology as the control cells and are well spread out, which suggests cell motility. After 4 days of incubation, the microscopy image remains similar to Figure 8d, except for a greater abundance of cells. Hence, whether the cells take up the P(PEGMA)-immobilized nanoparticles or not is not obvious from these microscopy images. The ICP-MS results below will provide clarification regarding this issue.

Cell viability is calculated from the number of cells incubated in the medium containing nanoparticles compared with that in the control experiment without nanoparticles. The viability of the cells after incubation in medium containing 0.2 mg/mL of pristine and P(PEGMA)-immobilized nanoparticles is compared in Figure 9. The viability of the cells incubated with P(PEGMA)-immobilized nanoparticles remained at >93% relative to the control during the period of incubation. This indicates that the P(PEGMA)-immobilized nanoparticles impart no cytotoxic effects to cells at a concentration of 0.2 mg/mL. On the other hand, when the cells were incubated with pristine nanoparticles, 30% loss in viability was observed in the first 2 days. The viability gradually increased in the next 3 days to about 90% in the fifth day. This decrease in cytotoxicity with incubation time can be attributed to the decrease in the concentration of nanoparticles in each macrophage cell. At the beginning, the macrophage cells were almost covered with nanoparticles (Figure 8b), and nanoparticles were being taken up by the cells. With the progressive cell division, the amount of nanoparticles in each cell will gradually decrease (Figure 8c) and the cytotoxic effects of the nanoparticles will diminish.

The extent of magnetic nanoparticles uptake by macrophage cells after incubation in the medium containing pristine and P(PEGMA)-immobilized nanoparticles was tested using ICP-MS. Figure 10 shows that the amount of pristine magnetic nanoparticles internalized into the cells normalized by the number of cells decreased from 154 pg/cell in the first day to 58 pg/cell after 5 days of incubation. This decrease is clearly due to the increase in the number of cells. These values were much higher than that reported for the uptake of 10 nm nanoparticles prepared via coprecipitation of Fe^{2+} and Fe^{3+} by addition of ammonia solution in aqueous solution.[39] For these particles, the uptake ranged from 4 to 12 pg/cell. This difference in uptake is due to the different surface properties of the nanoparticles obtained under different synthetic conditions. The presence of OH and NH_2 on the surface of these nanoparticles help them disperse in aqueous solution and decrease the aggregation.[39,40] On the other hand, the OH groups on surface of nanoparticles synthesized via high-temperature organic phase decomposition method used in the present work decreased greatly as the nanoparticles were heated to a high temperature (300 °C), and the alkane chains of the oleic acid on the nanoparticle surface increases its hydrophobicity. Both factors account for the higher uptake of pristine magnetic nanoparticles observed in the present work. The uptake of P(PEGMA)-immobilized nanoparticles by macrophage cells was less than 2 pg/cell during the 5 days (Figure 10b). This vast reduction in uptake is attributed to the fact that PEG side chains prevent the nanoparticles from aggregation, increase their resistance to the adsorption of proteins from the culture medium, and decrease their interaction with proteins on macrophage cells membrane.

In the body, the macrophages of the mononuclear phagocyte system are widely distributed and strategically placed to recognize and clear invading microorganisms or particles.[41] As such, injected nanoparticles face rapid elimination from the blood system due to the clearing action of the macrophages. The clearance mechanism by the macrophage cells is reported to comprise the following two steps:[41] plasma proteins first adsorb onto the surface of the nanoparticles and these proteins are capable of interacting with the specialized plasma membrane receptors on macrophages, thus promoting particle recognition by these cells. The endocytosis/phagocytosis of these particles by the macrophage cells would then follow. Therefore, the adsorption of the proteins onto the particle surface plays a key role during the clearance process. In our work, we have utilized P(PEGMA) immobilization onto the nanoparticle surface in

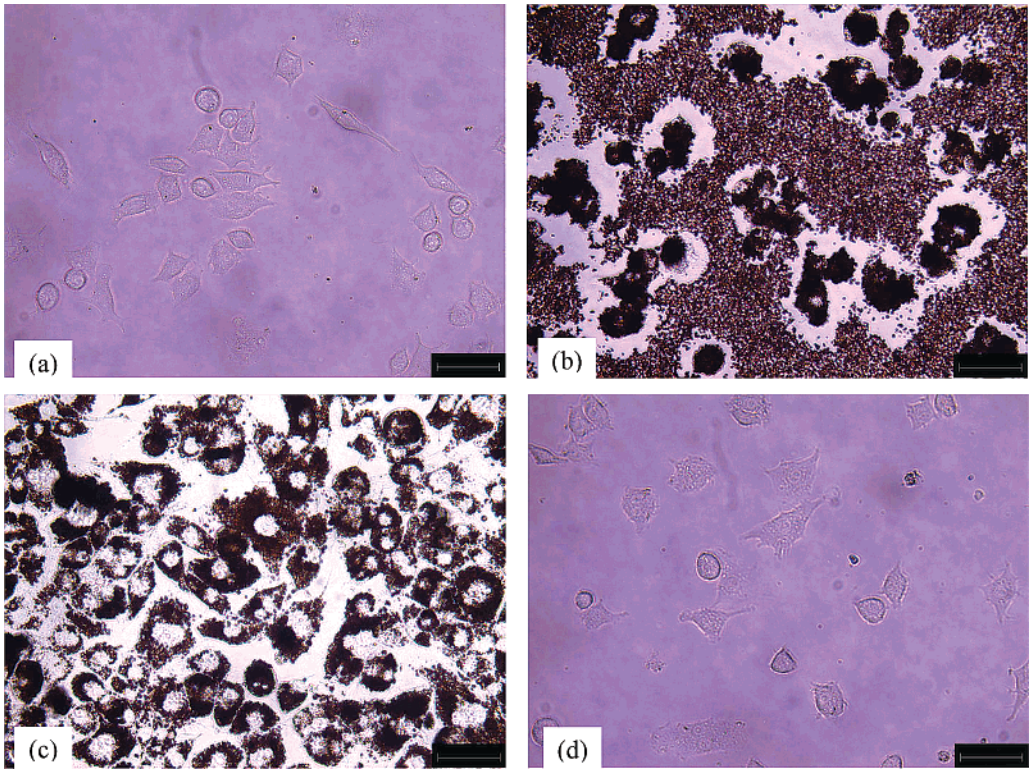

Figure 8. (a) RAW 264.7 cells in control culture (without any nanoparticles) after 1 day, (b) cells after culturing in medium containing pristine magnetic nanoparticles (0.2 mg/mL) for 1 day and (c) for 4 days, and (d) cells after culturing in medium containing P(PEGMA)-immobilized nanoparticles (0.2 mg/mL) for 1 day. The P(PEGMA)-immobilized nanoparticles were obtained after polymerization time of 2 h. Scale bar = 40 μm.

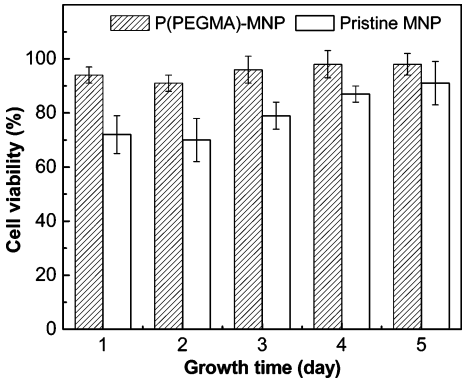

Figure 9. Viability of the macrophage cells cultured in medium containing 0.2 mg/mL magnetic nanoparticles. Cell viability is expressed relative to the cells in the control experiment without any nanoparticles.

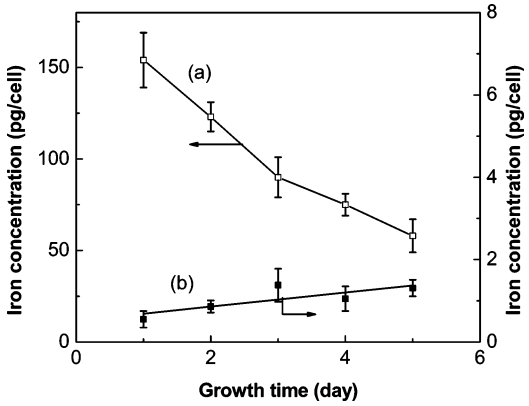

Figure 10. Iron concentration in RAW 264.7 cells cultured in medium containing (a) pristine magnetic nanoparticles and (b) P(PEGMA)-immobilized nanoparticles obtained after polymerization time of 2 h.

order to prevent proteins and macromolecules from depositing on the surface. The P(PEGMA) renders the surface neutral and hydrophilic. At the same time, the PEG side chains of the P(PEGMA) are highly flexible in aqueous solution, and if the macromolecules come close to the surface, the conformational degree of freedom for the polymer will be dramatically reduced resulting in an entropic repulsion between the surface and the macromolecules.[11]

4. Conclusion

A new method for PEGylation of magnetic nanoparticles was successfully carried out in this work. The magnetic nanoparticles were first modified with the CTS initiator, and PEGMA was then grafted onto the surface of magnetic nanoparticle via copper-mediated ATRP. The grafted P(PEGMA) chains are stable and enable the modified magnetic nanoparticles to disperse well in aqueous solutions. Moreover, the uptake of the magnetic nanoparticles by macrophage cells is greatly reduced after surface grafting with P(PEGMA). The morphology and viability of the macrophge cells cultured in a medium containing 0.2 mg/mL of P(PEGMA)-immobilized magnetic nanoparticles were similar to those of the cells in the control experiment without any nanoparticles. The uptake of nanoparticles by the macrophage cells was greatly reduced from 158 pg/cell to <2 pg/cell after grafting with P(PEGMA). This method provides opportunities for grafting a dense layer of hydrophilic polymer brushes onto the magnetic nanoparticles surface, and the preserved active chlorine groups and the −OH pendant groups of the P(PEGMA) can serve as reactive sites for further functionalization with target agents.

References and Notes

(1) Yan, F.; Xu, H.; Anker, J.; Kopelman, R.; Ross, B.; Rehemtulla, A.; Reddy, R. *J. Nanosci. Nanotechnol.* **2004**, *4*, 72−76.
(2) Perez, J. M.; Simeone, F. J.; Tsourkas, A.; Josephson, L.; Weissleder, R. *Nano Lett.* **2004**, *4*, 119−122.
(3) Lacava, L. M.; Lacava, Z. G. M.; Da Silva, M. F.; Silva, O.; Chaves, S. B.; Azevedo, R. B.; Pelegrini, F.; Gansau, C.; Buske, N.; Sabolovic, D.; Morais, P. C. *Biophys. J.* **2001**, *80*, 2483−2486.
(4) Bulte, J. W. M.; de Cuyper, M.; Despres, D.; Frank, J. A. *J. Magn. Magn. Mater.* **1999**, *194*, 204−209.
(5) Hafeli, U. O. *Int. J. Pharm.* **2004**, *277*, 19−24.
(6) Lubbe, A. S.; Bergemann, C.; Riess, H.; Schriever, F.; Reichardt, P.; Possinger, K.; Matthias, M.; Dorken, B.; Herrmann, F.; Gurtler, R.; Hohenberger, P.; Haas, N.; Sohr, R.; Sander, B.; Lemke, A. J.; Ohlendorf, D.; Huhnt, W.; Huhn, D. *Cancer Res.* **1996**, *56*, 4686−4693.
(7) Hafeli, U.; Schutt, W.; Teller, J.; Zborowski, M. *Scientific and Clinical Applications of Magnetic Carriers*, 1st ed.; Plenum Press: New York, 1997.
(8) Moroz, P.; Jones, S. K.; Gray, B. N. *Int. J. Hyperthermia* **2002**, *18*, 267−284.
(9) Allemann, E.; Gurny, R.; Doelker, E. *Eur. J. Pharm. Biopharm.* **1993**, *39*, 173−191.
(10) Zhang, M. Q.; Desai, T.; Ferrari, M. *Biomaterials* **1998**, *19*, 953−960.
(11) Harris, J. M.; Zalipsky, S. *Poly(ethylene glycol): chemistry and biological applications*; American Chemical Society: Washington, DC, 1997.
(12) Zhang, Y.; Kohler, N.; Zhang, M. Q. *Biomaterials* **2002**, *23*, 1553−1561.
(13) Kohler, N.; Fryxell, G. E.; Zhang, M. Q. *J. Am. Chem. Soc.* **2004**, *126*, 7206−7211.
(14) Gupta, A. K.; Gupta, M. *Biomaterials* **2005**, *26*, 3995−4021.
(15) Zhao, B.; Brittain, W. J. *Prog. Polym. Sci.* **2000**, *25*, 677−710.
(16) Vestal, C. R.; Zhang, Z. J. *J. Am. Chem. Soc.* **2002**, *124*, 14312−14313.
(17) Wang, Y.; Teng, X. W.; Wang, J. S.; Yang, H. *Nano Lett.* **2003**, *3*, 789−793.
(18) Li, G. F.; Fan, J. D.; Jiang, R.; Gao, Y. *Chem. Mater.* **2004**, *16*, 1835−1837.
(19) Marutani, E.; Yamamoto, S.; Ninjbadgar, T.; Tsujii, Y.; Fukuda, T.; Takano, M. *Polymer* **2004**, *45*, 2231−2235.
(20) Tao, L.; Mantovani, G.; Lecolley, F.; Haddleton, D. M. *J. Am. Chem. Soc.* **2004**, *126*, 13220−13221.
(21) Lecolley, F.; Tao, L.; Mantovani, G.; Durkin, I.; Lautru, S.; Haddleton, D. M. *Chem. Commun.* **2004**, 2026−2027.
(22) Xu, F. J.; Li, Y. L.; Kang, E. T.; Neoh, K. G. *Biomacromolecules* **2005**, *6*, 1759−1768.
(23) Chen, Y. W.; Ying, L.; Yu, W. H.; Kang, E. T.; Neoh, K. G. *Macromolecules* **2003**, *36*, 9451−9457.
(24) Li, Y. L.; Neoh, K. G.; Cen, L.; Kang, E. T. *Biotechnol. Bioeng.* **2003**, *84*, 305−313.
(25) Sun, S. H.; Zeng, H.; Robinson, D. B.; Raoux, S.; Rice, P. M.; Wang, S. X.; Li, G. X. *J. Am. Chem. Soc.* **2004**, *126*, 273−279.
(26) Binh, V. T.; Purcell, S. T.; Semet, V.; Feschet, F. *Appl. Surf. Sci.* **1998**, *132*, 803−814.
(27) Kuperman, V. *Magnetic Resonance Imaging: Physical Principles and Applications*; Academic Press: San Diego, 2000.
(28) Schwertmann, U.; Cornell, R. M. *Iron oxides in the laboratory: preparation and characterization*; VCH: Weinheim, Cambridge, 1991.
(29) Gupta, A. K.; Curtis, A. S. G. *Biomaterials* **2004**, *25*, 3029−3040.
(30) Pouchert, C. J. *The Aldrich Library of FT-IR Spectra*, 2nd ed.; Aldrich Chemical Co., Inc.: Milwaukee, 2001.
(31) Vestal, C. R.; Zhang, Z. J. *J. Am. Chem. Soc.* **2003**, *125*, 9828−9833.
(32) von Werne, T.; Patten, T. E. *J. Am. Chem. Soc.* **2001**, *123*, 7497−7505.
(33) Lu, H. C.; Yi, G. S.; Zhao, S. Y.; Chen, D. P.; Guo, L. H.; Cheng, J. *J. Mater. Chem.* **2004**, *14*, 1336−1341.
(34) Tartaj, P.; Serna, C. J. *J. Am. Chem. Soc.* **2003**, *125*, 15754−15755.
(35) Xu, C.; Xu, K.; Gu, H.; Zhong, X.; Guo, Z.; Zheng, R.; Zhang, X.; Xu, B. *J. Am. Chem. Soc.* **2004**, *126*, 3392−3393.
(36) Brusentsov, N. A.; Gogosov, V. V.; Brusentsova, T. N.; Sergeev, A. V.; Jurchenko, N. Y.; Kuznetsov, A. A.; Kuznetsov, O. A.; Shumakov, L. I. *J. Magn. Magn. Mater.* **2001**, *225*, 113−117.
(37) Mikhaylova, M.; Kim, D. K.; Bobrysheva, N.; Osmolowsky, M.; Semenov, V.; Tsakalakos, T.; Muhammed, M. *Langmuir* **2004**, *20*, 2472−2477.
(38) Zalipsky, S. *Bioconjugate Chem.* **1995**, *6*, 150−165.
(39) Qu, S. C.; Yang, H. B.; Ren, D. W.; Kan, S. H.; Zou, G. T.; Li, D. M.; Li, M. H. *J. Colloid. Interface. Sci.* **1999**, *215*, 190−192.
(40) Huang, S. H.; Liao, M. H.; Chen, D. H. *Biotechnol. Prog.* **2003**, *19*, 1095−1100.
(41) Mornet, S.; Vasseur, S.; Grasset, F.; Duguet, E. *J. Mater. Chem.* **2004**, *14*, 2161−2175.

BM050870E